Noise sources and improved performance of a mid-wave infrared uncooled silicon carbide optical photodetector

Geunsik Lim,[1] Tariq Manzur,[2] and Aravinda Kar[1,*]

[1]Laser-Advanced Materials Processing Laboratory, Department of Mechanical, Materials and Aerospace Engineering,
College of Optics and Photonics, Center for Research and Education in Optics and Lasers (CREOL),
University of Central Florida, Orlando, Florida 32816-2700, USA

[2]S&T Lead, I&EW, Undersea Warfare Electromagnetic Systems Development, Building 1319,
1176 Howell Street, Newport, Rhode Island 02841-1708, USA

*Corresponding author: akar@creol.ucf.edu

Received 6 August 2014; revised 29 October 2014; accepted 6 November 2014;
posted 6 November 2014 (Doc. ID 220464); published 16 December 2014

An uncooled photon detector is fabricated for the mid-wave infrared (MWIR) wavelength of 4.21 μm by doping an n-type 4H-SiC substrate with gallium using a laser doping technique. The dopant creates a p-type energy level of 0.3 eV, which is the energy of a photon corresponding to the MWIR wavelength 4.21 μm. This energy level was confirmed by optical absorption spectroscopy. The detection mechanism involves photoexcitation of carriers by the photons of this wavelength absorbed in the semiconductor. The resulting changes in the carrier densities at different energy levels modify the refractive index and, therefore, the reflectance of the semiconductor. This change in the reflectance constitutes the optical response of the detector, which can be probed remotely with a laser beam such as a He–Ne laser and the power of the reflected probe beam can be measured with a conventional laser power meter. The noise mechanisms in the probe laser, silicon carbide MWIR detector, and laser power meter affect the performance of the detector in regards to aspects such as the responsivity, noise equivalent temperature difference (NETD), and detectivity. For the MWIR wavelengths of 4.21 and 4.63 μm, the experimental detectivity of the optical photodetector of this study was found to be $1.07 \times 10^{10}\ \mathrm{cm} \cdot \mathrm{Hz}^{1/2}/\mathrm{W}$, while the theoretical value was $1.11 \times 10^{10}\ \mathrm{cm} \cdot \mathrm{Hz}^{1/2}/\mathrm{W}$. The values of NETD are 404 and 15.5 mK based on experimental data for an MWIR radiation source with a temperature of 25°C and theoretical calculations, respectively.

OCIS codes: (040.0040) Detectors; (040.3060) Infrared; (040.6070) Solid state detectors.
http://dx.doi.org/10.1364/AO.53.008410

1. Introduction

Mid-wave infrared (MWIR) photon detectors operate in the wavelength range of 3 to 5 μm for a variety of applications including pollution detection, industrial process monitoring, chemical forensics, chemical and biological warfare, and noninvasive medical diagnostics [1–4]. Most such detectors are based on narrow bandgap semiconductor devices with excellent signal-to-noise ratios and very fast response times. In these devices, however, the dark current increases exponentially due to thermally generated charge carriers with increasing temperature. To suppress this type of noise, the cooling of semiconductor-based detectors such as photoconductors, photoelectromagnetic detectors, Dember effect detectors, and HgCdTe (MCT) photodiodes has been investigated for room temperature operations [5]. Uncooled infrared (IR) detectors such as thermocouples, pyroelectric and ferroelectric detectors, and microbolometers are currently available [6–9]. Much attention has been paid to fabricating uncooled IR detectors with other operating mechanisms such as the optomechanical IR

1559-128X/14/368410-14$15.00/0

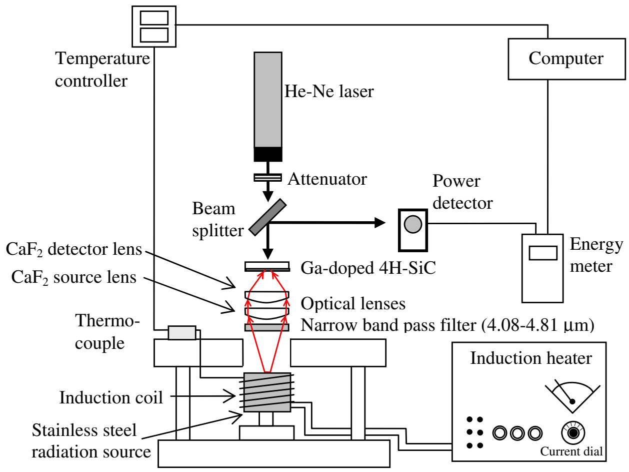

Fig. 1. Experimental setup for testing the optical response of the SiC detector at the MWIR wavelengths of 4.21 and 4.63 μm.

imaging system with a bimaterial microcantilever array [10–12].

Wide bandgap semiconductors such as SiC and GaN are another class of materials with the capability of high operating temperature and high frequency power amplification [13,14] that can be used for fabricating MWIR detectors. We have doped an n-type 4H-SiC substrate with Ga to produce an acceptor energy level of 0.30 eV that corresponds to the energy of a photon at the MWIR wavelength of 4.21 μm; therefore, the doped sample acts as an MWIR detector. The incident MWIR photons transfer carriers from the valence band to the acceptor level, which modifies the refractive index of the doped region because of the changes in the carrier density at these two energy levels. Consequently, the reflectivity of the doped region changes, and this change in the reflectance, which represents the optical response of the detector, is probed with a He–Ne laser beam as shown in Fig. 1. In this paper, the sources of noise due to different components of the detector are analyzed and the noise equivalent temperature difference (NETD) and detectivity are investigated.

2. Experimental Procedure

A. Measurement of the Detector Response

An n-type 4H-SiC substrate with a length, width, and thickness of 1, 1, and 0.0375 cm, respectively, were doped with Ga using a laser doping technique and the metallorganic precursor triethylgallium [$(C_2H_5)_3Ga$]. The precursor is decomposed at the laser-heated substrate surface without melting the substrate and the Ga atom diffuses into the substrate. The details of a typical laser doping apparatus are discussed elsewhere [15].

The optical properties of the Ga-doped sample, which was produced by scanning a certain region of the substrate with a laser beam, and the as-received 4H-SiC sample were measured using a Bruker Vertex 70 Fourier transform infrared (FTIR) spectrometer equipped with a Helios infrared micro-sampling accessory. The absorption spectra of the doped sample revealed a peak at 4.21 μm (0.30 eV) with 25% absorbance, which is higher than the 12% absorbance of the as-received sample as shown in Fig. 2(a). However, the doped sample exhibits another absorption peak at the 4.63 μm (0.27 eV) wavelength. This peak will also contribute to the detector response since a narrow bandpass filter of transmission range 4.08–4.81 μm is used in this study to extract the MWIR wavelengths from a broadband source of electromagnetic (EM) waves. The doped sample has higher absorption coefficient than the as-received sample, which indicates that the Ga dopant has modified the optical properties of the as-received sample [16].

The doped sample exhibits a change in its reflectance depending on the irradiance of incident photons. This irradiance depends on the temperature of the source, which emits the photons of interest, and the radiation collection optics that collect the photons and focus them onto the detector. The optical response of the detector was tested using the setup presented in Fig. 1. Since the focal length of the CaF_2 lens (source lens) was 50 mm, it was placed 50 mm above the hot stainless steel radiation source and a narrow bandpass filter was positioned right below the lens. The filter had a high transmittance (~92.5%) in the range 4.08–4.81 μm and a sharp cut-off outside this band. Another CaF_2 lens (detector lens) was placed above the source lens so that the convex surfaces of both lenses face the incident wave to reduce spherical aberrations. A CW He–Ne laser beam of output power up to 15 mW was used as a probe laser. The power was reduced to 752 nW using an attenuator placed right below the laser to measure the optical response of the SiC detector. A silicon-based power meter was used at its lowest resolution (0.63 nW) to measure subtle changes in the power of the reflected He–Ne beam.

3. Performance of the IR Detector

A. Effect of Photogenerated Carriers on the Reflectance of the Doped Region

Absorption of the incident photon energy by the doped sample creates photoexcited carriers due to the jumping of carriers from the valence band to the Ga dopant energy level. The change in the number density of carriers due to photoexcitation can be obtained from the following equation (see Appendix A) at any time t:

$$\frac{d(\Delta N_c)}{dt} = \frac{I_a \eta_{i,\mathrm{SiC}} A_{\mathrm{SiC}}}{h\nu_M V} - \Delta N_c\left(\frac{1}{\tau_r} + \frac{1}{d_d}\sqrt{\frac{D}{4\tau_d}}\right), \qquad (1)$$

where the first term on the right hand side is the rate of photogeneration of carriers within the doped region of area A_{SiC} at the SiC substrate surface and depth d_d inside the substrate, and the second and third terms are the rates of carrier density loss

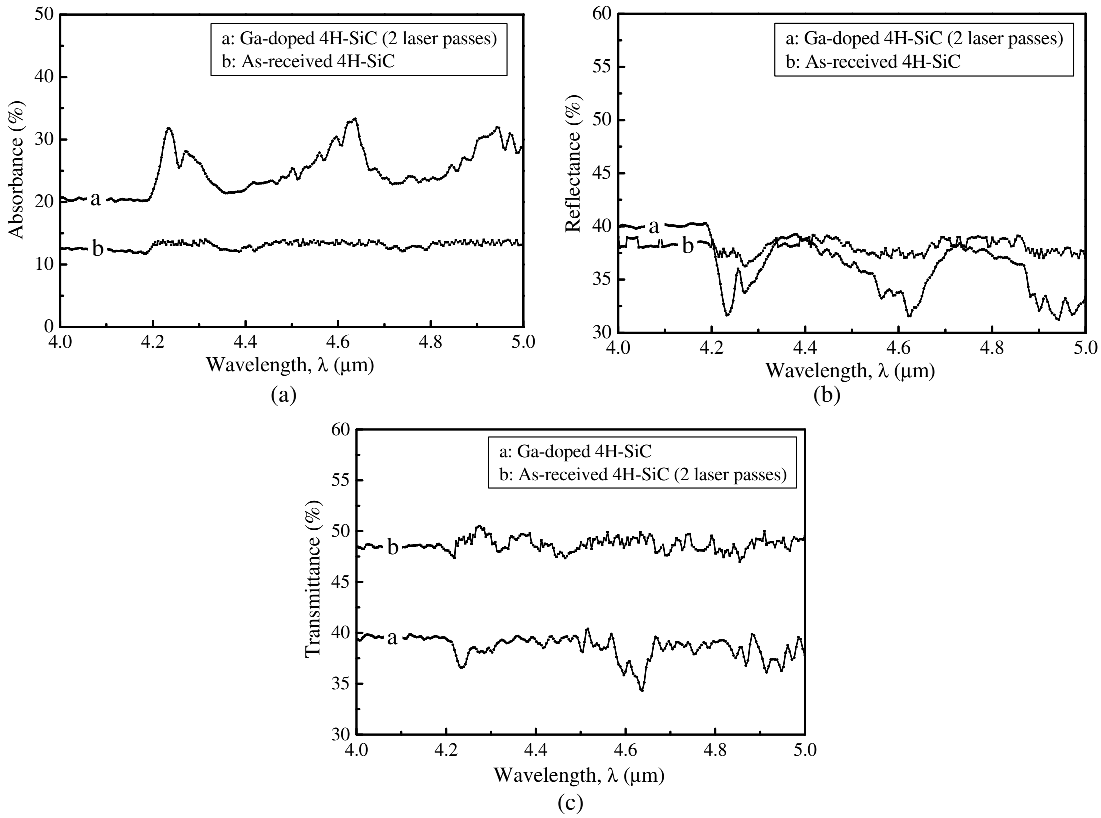

(a) (b) (c)

Fig. 2. Spectroscopic data showing the optical properties of as-received 4H-SiC and Ga-doped 4H-SiC (two-pass samples where indicated): (a) absorbance, (b) reflectance, and (c) transmittance in the wavelength range 4–5 μm.

due to recombination and diffusion of carriers from the photoexcited region, respectively. Here, ΔN_c is the change in the number of carriers at the photoexcited state per unit volume of the doped region, V. $\eta_{i,\mathrm{SiC}}$ and h are the internal quantum efficiency of the SiC detector and Planck's constant, respectively, and ν_M is the frequency of the MWIR radiation. τ_r is the recombination time, i.e., the lifetime of the carriers at the photoexcited state, D is the diffusivity of the photoexcited carriers, and τ_d is the characteristic diffusion time. I_a is the absorbed irradiance of the MWIR radiation from the finite source, which can be expressed as [4] $I_a = \alpha_{\mathrm{SiC}} \varepsilon_s (L_B)_{\lambda_{12}} (\tau_0 / 4F^2)$, where α_{SiC} is the absorbance of the doped sample for the MWIR wavelength λ. The absorbance is determined by considering multiple reflections inside the sample. ε_s and τ_0 are the emissivity of the radiation source and the transmissivity of the radiation collection optics (e.g., lens and filter), respectively. F is the f-number of the detector lens. L_B is the spectral radiance of the blackbody source. $(L_B)_{\lambda_{12}} = (L_B)_{\lambda_1} + (L_B)_{\lambda_2}$, where $(L_B)_{\lambda_1}$ and $(L_B)_{\lambda_2}$ are the radiances due to the emission bands centered around two MWIR wavelengths $\lambda_1 = 4.21$ μm and $\lambda_2 = 4.63$ μm, respectively. These two wavelengths are considered because they represent two absorbance peaks of the detector [Fig. 2(a)] and the filter of this study transmits them from the radiation source to the detector.

Equation (1) yields the following expression for the change in the photoexcited carrier density at steady state [17]:

$$\Delta N_c = \frac{I_a \eta_{i,\mathrm{SiC}} \tau_r \sqrt{4\tau_d}}{\left(d_d \sqrt{4\tau_d} + \tau_r \sqrt{D}\right) h\nu_M}. \tag{2}$$

Another optical effect is the interference due to multiple reflections of the He–Ne laser probe beam and the MWIR radiation in the doped and undoped regions of the detector, which increases the absorption of photons in the sample. The Ga-doped sample has three interfaces between the air and doped region, the doped region and undoped silicon carbide, and the undoped silicon carbide and air. The reflectance due to multiple reflections at these interfaces can be expressed as [18]

$$\begin{aligned}\rho_{\mathrm{SiC}} = {} & R_{au} + R_{du}(1 - R_{au})^2 e^{-2\mu_u d_u} \\ & + \frac{R_{du}^2 R_{au} (1 - R_{au})^2 e^{-4\mu_u d_u}}{1 - R_{du} R_{au} e^{-2\mu_u d_u}} \\ & + (1 - R_{au})^2 (1 - R_{du})^2 R_{du} e^{-2\mu_u d_u} e^{-2\mu_d d_d} \\ & + \frac{(1 - R_{au})^2 (1 - R_{du})^2 R_{au} R_{ad} R_{du} e^{-4\mu_u d_u} e^{-2\mu_d d_d}}{1 - R_{au} R_{du} e^{-2\mu_u d_u}},\end{aligned} \tag{3}$$

where ρ_{SiC} is the reflectance of the doped SiC sample at the He–Ne laser wavelength in the presence of MWIR irradiance on the sample. R_{au}, R_{du}, and R_{ad} are the reflectivities at the interfaces between the air and undoped region, the doped and undoped regions, and the air and doped region, respectively. The absorption coefficients and thicknesses of the doped and undoped regions are denoted by μ_d and μ_u, and d_d and d_u, respectively.

The reflectance is a function of the reflectivity and absorption coefficient. Since refractive and absorption indices depend on the free carrier density and reflectivity depends on the refractive and absorption indices, the reflectivity is ultimately affected by the free carrier density. Similarly, the absorption coefficient, which depends on the absorption index, is ultimately affected by the free carrier density since the absorption index is a function of the free carrier density. Because of this functional dependence of the optical properties on the free carrier density, the reflectance of the detector will depend on the free carrier density. Therefore, the noise in the free carrier density will affect the performance of the optical detector.

4. Noise Sources in the Silicon Carbide Detector

The response of any detector system is severely affected by the noise of its different components. In the SiC optical photodetector, noise may arise from a variety of effects such as the interaction of the SiC detector with the incident photons from the source, noise mechanisms due to the interaction between the He–Ne laser and SiC detector, the fluctuation in the reflected power of the He–Ne beam arriving at the Si detector, and the noise of the Si detector itself.

A. Noises in the SiC Detector

The noises in the Ga-doped 4H-SiC detector are the photon shot noise, Johnson noise, and the carrier generation–recombination noise. When photons strike a detector, the photon-detector interactions immediately produce a signal variance or noise due to the fluctuations in the number of photons emitted by the source and the randomness in the production of photoexcited carriers. The mean square noise of the photoexcited carrier density can be written as [4]

$$\langle \delta N_{c,Q}^2 \rangle^{1/2} = \frac{l_D}{4D}\left[\frac{\eta_{i,\mathrm{SiC}}\alpha_{\mathrm{SiC}}\varepsilon_s\tau_0\Delta f_{\mathrm{SiC}}}{4F^2A_{\mathrm{SiC}}h\nu_M}(L_B)_{\lambda_{12}}\right]^{1/2}, \quad (4)$$

where l_D is the characteristic diffusion length of the carrier in the detector and Δf_{SiC} is the noise bandwidth of the Ga-doped 4H-SiC detector.

The Johnson noise is the fluctuation of the photoexcited carriers due to their thermal motions, and the mean square of this noise can be written as [4]

$$\langle \delta N_{c,J}^2 \rangle^{1/2} = \frac{l_D}{2A_{\mathrm{SiC}}Dq}\sqrt{\frac{k_B T_{\mathrm{SiC}}\Delta f_{\mathrm{SiC}}}{R_{e,\mathrm{SiC}}}}, \quad (5)$$

where k_B and T_{SiC} are the Boltzmann constant and the temperature of the Ga-doped SiC detector, respectively. q is the charge of a carrier and $R_{e,\mathrm{SiC}}$ is the electrical resistivity of the detector.

The carrier generation–recombination noise arises from statistical fluctuations in the rate of photoexcitation of carriers from the valence band to the dopant energy level and the rate of relaxation of these photoexcited carriers from the dopant energy level to the valence band. The mean square of this noise, assuming thermally generated free carriers are insignificant, can be written as [4]

$$\langle \delta N_{c,GR}^2 \rangle^{1/2} = \frac{l_D^3}{8\tau_r D^2}\left[\frac{\eta_{i,\mathrm{SiC}}\alpha_{\mathrm{SiC}}\varepsilon_s\tau_0\Delta f_{\mathrm{SiC}}}{4F^2A_{\mathrm{SiC}}h\nu_M}(L_B)_{\lambda_{12}}\right]^{1/2}. \quad (6)$$

B. Interferometric Noise due to Interaction between the He–Ne Laser and SiC Detector

Interference occurs because of the multiple reflections of the He–Ne laser beam as it propagates inside the SiC detector. Therefore, the reflected power of the He–Ne laser can have interferometric noise, which represents the phase of the laser varying randomly as a function of time. The laser has random phase fluctuations at the exit of the laser system. These phases are modified further as the laser beam travels through different optical paths inside the SiC detector, and this causes fluctuations in the power of the He–Ne laser reflected by the detector, i.e., a random signal is produced by the detector. The characteristics of the interferometer, which is the detector itself in the present case, are determined by the reflectivities at different interfaces inside the detector and the delay time, τ, for the arrival of the laser wavefronts to the interfaces of the SiC detector. The spectral density of the interferometric noise due to multiple reflections can be expressed as [19]

$$\begin{aligned}\mathrm{RIN}(\nu_L) &= \frac{4r^2}{\pi}\left[\frac{\Delta\nu}{\nu_L^2+(\Delta\nu)^2}\right] \\ &\times\Big[\sin^2(\omega_0\tau)\{1+e^{-4\pi\Delta\nu\tau}-2e^{-2\pi\Delta\nu\tau}\cos(2\pi\nu_L\tau)\} \\ &+\cos^2(\omega_0\tau)\left\{1-e^{-4\pi\Delta\nu\tau}-2e^{-2\pi\Delta\nu\tau}\frac{\Delta\nu}{\nu_L}\sin(2\pi\nu_L\tau)\right\}\Big],\end{aligned} \quad (7)$$

where the RIN is the relative intensity noise that represents the amount of noise relative to the magnitude of signal. It will be discussed more detail in next section. r is an effective reflection coefficient, which depends on the reflection coefficients of various interfaces of the detector. $\Delta\nu$, ν_L, and ω_0 are the linewidth in frequency units, the frequency of the He–Ne laser, and the center angular frequency of the He–Ne laser, respectively. It can be shown from Eq. (7) that $\mathrm{RIN}(\nu_L)$ is maximum, i.e., the conversion of the incident laser phase noise into the reflected laser intensity (signal) noise is maximum, when $\omega_0\tau = (n + 1/2)\pi$ for $n = 1, 2, 3, \ldots$. However, for a shorter delay time, in the limit of $2\pi\tau\Delta\nu \ll 1$, which holds good in the present case for the He–Ne laser of linewidth $\Delta\nu = 310$ MHz and the delay time $\tau = 9.75$ ps, Eq. (7) simplifies to the following expression for $\mathrm{RIN}(\nu_L)$:

$$\mathrm{RIN}(\nu_L) = \frac{16}{\pi} r^2 \Delta\nu \tau^2 \operatorname{sinc}^2(\nu_L \tau), \tag{8}$$

where the sinc function is defined by $\operatorname{sinc}(x) = (\sin x/x)$. Small phase fluctuations occur in lasers with very narrow linewidth, and this results in less interferometric intensity noise. Based on the reflectivities R_{au}, R_{du}, and R_{ad}, the effective reflection coefficient, r, is determined from the following expression [19]:

$$\begin{aligned} r(t,\tau) = {} & 2\left(1 - \sqrt{R_{au}}\right)^4 R_{au} R_{du} \\ & \times \begin{cases} e^{-2\pi\Delta f|t|}[1 + \cos(2\omega_0\tau_1) e^{-4\pi\Delta f(\tau_1 - |t|)}], & |t| < \tau_1 \\ e^{-2\pi\Delta f\tau_1}[1 + \cos(2\omega_0\tau_1)], & |t| > \tau_1 \end{cases} \\ & + 2\left(1 - \sqrt{R_{au}}\right)^4 \left(1 - \sqrt{R_{du}}\right)^4 R_{au} R_{ad} \\ & \times \begin{cases} e^{-2\pi\Delta f|t|}[1 + \cos(2\omega_0\tau_2) e^{-4\pi\Delta f(\tau_2 - |t|)}], & |t| < \tau_2 \\ e^{-2\pi\Delta f\tau_2}[1 + \cos(2\omega_0\tau_2)], & |t| > \tau_2 \end{cases}, \end{aligned} \tag{9}$$

where τ_1 and τ_2 are the delay times given by $\tau_1 = 2d_u n_u/c \cos(\theta_{t1})$ and $\tau_2 = 2d_d n_d/c \cos(\theta_{t2}) + d_u n_u/c \cos(\theta_{t1})$, where c is the speed of light in vacuum. θ_{t1} and θ_{t2} are the angle of He–Ne laser transmission axis from the normal direction of the undoped and doped samples, respectively.

Using Eqs. (8) and (9), the reflected He–Ne laser power noise due to intensity fluctuations can be written as

$$\langle \delta P_{r,I}^2 \rangle^{1/2} = P_L \sqrt{16\pi\left(1 - \sqrt{R_{au}}\right)^4 R_{au} \Delta\nu \left(R_{du}\tau_1 + \left(1 - \sqrt{R_{du}}\right)^4 R_{ad}\tau_2\right)}, \tag{10}$$

where P_L is the incident power of the He–Ne laser. Equation (10) is used in Section 4.E to calculate $\mathrm{NETD_{Th}}$.

C. Noises in the He–Ne Laser Probe Beam

The phase noise fluctuations of a laser can produce intensity noise fluctuations [20]. The noises of a He–Ne laser are power noises due to the frequency and power fluctuations. Additionally, the interaction between the He–Ne laser and detector produces a noise in the reflected He–Ne laser power due to the fluctuations in the reflectance of the detector. The main noise mechanism for the laser is the spontaneous emission noise, which yields fluctuations in the emitted optical power and the emission frequency. The RIN represents the amount of noise relative to the magnitude of signal, which is given by $\sigma^2/\langle P \rangle^2$, where σ is the standard deviation of the noise distribution, i.e., σ^2 is the noise variance and $\langle P \rangle$ is the average power of the signal. The total RIN is expressed in terms of power as [21]

$$\mathrm{RIN_{total}}(t) = \frac{\langle \delta P(t)^2 \rangle}{\langle P(t) \rangle^2}, \tag{11}$$

where $\delta P(t)$ is the intensity fluctuation of laser. Based on the spectral density of RIN in the optical frequency domain (ν_L), which is denoted by RIN (ν_L), the total RIN over all frequencies can also be written as [22]

$$\mathrm{RIN_{total}} = \int_{-\infty}^{\infty} \mathrm{RIN}(\nu_L) \mathrm{d}\nu_L. \tag{12}$$

In terms of the reflected power fluctuations, $\delta P(t)$, in the oscillator cavity of the He–Ne laser, the Fourier transform of the autocorrelation function of $\delta P(t)$ leads to a spectral density of the square of the power fluctuations in units of $\mathrm{W^2/Hz}$, which is denoted by $\mathrm{W}_{\Delta P}(\nu_L)$. The corresponding spectral density of RIN is given by $\mathrm{RIN}(\nu_L) = W_{\Delta P}(\nu_L)/\langle P \rangle^2$ with

$$W_{\Delta P}(\nu_L) = \frac{\eta_{e,L} \hbar \omega_m P_L \Delta\rho_{\mathrm{SiC},L}}{\pi t_p^2 (\nu_L^2 + \omega_1^2)},$$

where $\hbar$ is the reduced Planck constant, ω_m is the modulated angular frequency of the laser, i.e., the bandwidth of the He–Ne laser around its nominal angular frequency ω_1, $\eta_{e,L}$ is the external quantum efficiency of the laser, P_L is the average power of the laser beam, and t_p is the pulse width at the half-intensity points of the laser [21,22]. Similarly, in terms of frequency fluctuations, the spectral density of RIN is given by $\mathrm{RIN}(\nu_L) = 4\pi^2\tau^2 \mathrm{W}_{\Delta\omega}(\nu_L)$ corresponding to the spectral density of frequency noise

$$W_{\Delta\omega}(\nu_L) = \frac{\eta_{e,L} \hbar \omega_m}{P_L \Delta\rho_{\mathrm{SiC},L}} \frac{\beta^2 \omega_1^2}{4\pi t_p^2 (\nu_L^2 + \omega_1^2)},$$

where β is the phase-amplitude coupling constant that is caused by the variation in the carrier density.

The carrier density in various energy levels of the He–Ne laser gain medium may vary because of the thermal drift of the gain medium and input electrical power fluctuation. Because of the variation of carrier density, the amplitude and frequency of the lasing optical field fluctuate. This fluctuating field alters the phase and intensity of the He–Ne laser and broadens the laser linewidth [21]. Using these expressions and Eqs. (11) and (12), the reflected He–Ne laser power noises due to the power and frequency fluctuations, respectively, can be written as

$$\langle \delta P_{L,P}^2 \rangle^{1/2} = \sqrt{\frac{\pi \eta_{e,L} P_L h\nu_L}{t_p^2 \omega_1}} \tag{13}$$

and

$$\langle \delta P_{L,F}^2 \rangle^{1/2} = \sqrt{\frac{\pi \eta_{e,L} P_L h\nu_L \alpha_{\mathrm{SiC},L}^2 \tau^2 \omega_1}{2t_p^2}}, \tag{14}$$

where $\alpha_{\mathrm{SiC},L}$ is the absorbance of the SiC detector at the He–Ne laser wavelength. Equations (13) and (14) are used in Section 4.E to calculate the theoretical $\mathrm{NETD_{Th}}$.

D. Noise due to the He–Ne Laser Detector (Si-based Photodetector)

The noise mechanisms in the Si detector are the photon shot noise caused by the He–Ne laser photons that are incident on the Si detector after being reflected by the SiC detector, as well as the Johnson, shot, and generation–recombination noises due to the He–Ne laser photon-induced electrons in the Si detector. The photon shot noise due to the He–Ne laser is [4]

$$\langle \delta i_{\mathrm{Si},Q}^2 \rangle^{1/2} = q\sqrt{\frac{\eta_{e,\mathrm{Si}} P_L \rho_{\mathrm{SiC},L} \Delta f_{\mathrm{Si}}}{h\nu_L}}, \tag{15}$$

where $\rho_{\mathrm{SiC},L}$ is the reflectance of the SiC detector for the He–Ne laser wavelength in the presence of MWIR irradiance. $\eta_{e,\mathrm{Si}}$ is the external quantum efficiency of the Si detector and Δf_{Si} is the noise bandwidth of the Si detector.

The Johnson or Nyquist noise describes the fluctuations in the voltage across a dissipative circuit element that are caused by the thermal motion of the charge carriers. The charge neutrality is satisfied in an electrical element (e.g., resistor) when considering the whole volume, but locally the random thermal motion of the carriers sets up fluctuating charge gradients and, therefore, a fluctuating voltage. The noise due to this thermal motion can be expressed as [4]

$$\langle \delta i_{\mathrm{Si},J}^2 \rangle^{1/2} = \sqrt{\frac{4k_B T_{\mathrm{Si}} \Delta f_{\mathrm{Si}}}{R_{e,\mathrm{Si}}}}, \tag{16}$$

where T_{Si} and $R_{e,\mathrm{Si}}$ are the temperature and the electrical resistivity of the Si detector, respectively.

The current arising from random generation and flow of mobile charge carriers is identified with the shot noise. This shot noise is caused by the fluctuations in the current due to the discreteness of the charge carriers, and the random electronic emission for which the number of electrons emitted per unit time obey Poisson statistics, yields the following expression for the shot noise [4]:

$$\langle \delta i_{\mathrm{Si},S}^2 \rangle^{1/2} = \sqrt{2q \langle \delta i_{\mathrm{Si},Q}^2 \rangle^{1/2} \Delta f_{\mathrm{Si}}}. \tag{17}$$

The generation–recombination noise, which addresses the population of charge carriers in an excited state and the transition of the carriers from the excited state to their ground state, is given by [4]

$$\langle \delta i_{\mathrm{Si},GR}^2 \rangle^{1/2} = 2qG\sqrt{\eta_{e,\mathrm{Si}} \frac{P_L \rho_{\mathrm{SiC},L}}{h\nu_L} \Delta f_{\mathrm{Si}} + g_{\mathrm{th}} A_{\mathrm{Si}} \Delta f_{\mathrm{Si}} l_t}, \tag{18}$$

where G is the photoconductive gain. $g_{\mathrm{th}}, A_{\mathrm{Si}}$, and l_t are the thermal generation of carriers, the area of the Si detector, and the detector thickness, respectively.

E. Noise Equivalent Temperature Difference due to Various Noise Mechanisms

From the above noise sources in the SiC optical photodetector, the detector performance can be evaluated. The NETD is an important performance parameter of infrared imaging systems, and it is defined as the temperature difference between two adjacent points on the target source for which the difference in the detector signals is equal to the noise of the detector. For the NETD calculation of the SiC detector, the signal term is denoted by $\Delta N_c(T_s)$, which is the difference in the free carrier density of the doped sample in the presence of the MWIR irradiation at a given temperature of the source T_s. When the source temperature varies from T_{s1} to T_{s2}, the detector signal is $\Delta N_c(T_s) = N_c(T_{s2}) - N_c(T_{s1})$. The noise equivalent power (NEP) is the incident infrared power on an infrared detector that generates a signal output (S) that is equal to the root-mean-square (RMS) noise output N, which results in a signal-to-noise ratio (S/N) of 1. The signal-to-noise ratio can be calculated using the following expression:

$$\frac{\Delta N_c}{\langle \delta N_c^2 \rangle^{1/2}} = \frac{\Delta T_s \eta_{i,\mathrm{SiC}} \tau_r \sqrt{4\tau_d}\left[\frac{\alpha_{\mathrm{SiC}} \varepsilon_s \tau_0}{4F^2}\left(\frac{dL_B}{dT_s}\right)_{\lambda_{12}}\right]}{h\nu_M (d_d \sqrt{4\tau_d} + \tau_r \sqrt{D})(\langle \delta N_{c,Q}^2 \rangle^{1/2} + \langle \delta N_{c,J}^2 \rangle^{1/2} + \langle \delta N_{c,GR}^2 \rangle^{1/2})}, \tag{19}$$

where $\langle \delta N_c^2 \rangle^{1/2}$ represents the noise for a given noise mechanism that consists of photon shot noise from the radiation source, Johnson noise, and generation–recombination noise. Since $\Delta T_s = \mathrm{NETD}$ at $S/N = 1$ by the definition of NETD as the temperature of the target for which the signal-to-noise ratio equals unity, the generalized expression for NETD of the doped SiC detector is

$$\mathrm{NETD}_{\mathrm{SiC}} = \frac{4F^2 h\nu_M \left(d_d \sqrt{4\tau_d} + \tau_r \sqrt{D}\right)\left(\langle \delta N_{c,Q}^2 \rangle^{1/2} + \langle \delta N_{c,J}^2 \rangle^{1/2} + \langle \delta N_{c,GR}^2 \rangle^{1/2}\right)}{\eta_{i,\mathrm{SiC}} \alpha_{\mathrm{SiC}} \varepsilon_s \tau_0 \tau_r \sqrt{4\tau_d} \left(\frac{dL_B}{dT_s}\right)_{\lambda_{12}}}. \tag{20}$$

The signal-to-noise ratio for the He–Ne laser beam and doped SiC detector due to interferometric noise caused by multiple reflection and interference can be calculated by $\Delta\rho_{\mathrm{SiC},L} / \langle \delta\rho_{\mathrm{SiC},L}^2 \rangle^{1/2} \equiv \Delta P_{r,L} / \langle \delta P_{r,I}^2 \rangle^{1/2}$. Since $\Delta T_{\mathrm{SiC}} = \mathrm{NETD}$ at $S/N = 1$, the generalized expression for NETD due to the interaction between the He–Ne laser and SiC detector is

$$\mathrm{NETD}_{L,\mathrm{SiC}} = \frac{\langle \delta P_{r,I}^2 \rangle^{1/2}}{\frac{dP_{r,L}}{dT_{\mathrm{SiC}}}}, \tag{21}$$

where $P_{r,L}$ is the reflected power of the He–Ne laser and T_{SiC} is the temperature of the SiC detector.

The NETD for the He–Ne laser and Si detector is determined using $\langle \delta P_{r,P}^2 \rangle^{1/2} + \langle \delta P_{r,F}^2 \rangle^{1/2}$, which represents the power noise due to intensity and frequency fluctuation in the reflected He–Ne laser beam arriving at the Si detector. Since $\Delta T_L = \mathrm{NETD}$ at $S/N = 1$, the generalized expression for NETD due to the fluctuation in the reflected power of the He–Ne beam arriving at the Si detector is

$$\mathrm{NETD}_{L,\mathrm{Si}} = \frac{\langle \delta P_{r,P}^2 \rangle^{1/2} + \langle \delta P_{r,F}^2 \rangle^{1/2}}{\frac{dP_L}{dT_L}}, \tag{22}$$

where T_L is the temperature of the He–Ne laser.

Since the He–Ne laser power noise can be measured as a current in the Si detector, the signal-to-noise ratio for the He–Ne laser power meter (Si detector) can be calculated by the ratio $\Delta i_{\mathrm{Si}} / \langle \delta i_{\mathrm{Si}}^2 \rangle^{1/2}$. The noise sources are photon shot noise from the He–Ne laser as well as Johnson, shot, and generation–recombination noises. Since $\Delta T_{\mathrm{Si}} = \mathrm{NETD}$ at $S/N = 1$, the generalized expression for NETD of the Si detector itself is

$$\mathrm{NETD}_{\mathrm{Si}} = \frac{h\nu_L}{q\eta_{i,\mathrm{Si}} \alpha_{\mathrm{Si}}} \frac{\langle \delta i_{\mathrm{Si}}^2 \rangle^{1/2}}{\frac{dP_{r,L}}{dT_{\mathrm{SiC}}}}, \tag{23}$$

where $\eta_{i,\mathrm{Si}}$ and α_{Si} are the internal quantum efficiency and absorbance of the Si detector at the He–Ne laser wavelength. Therefore, taking into account all the fundamental noise sources described above, the total theoretical NETD can be obtained by $\mathrm{NETD}_{\mathrm{Th}} = \sqrt{\mathrm{NETD}_{\mathrm{SiC}}^2 + \mathrm{NETD}_{L,\mathrm{SiC}}^2 + \mathrm{NETD}_{L,\mathrm{Si}}^2 + \mathrm{NETD}_{\mathrm{Si}}^2}$ [23].

F. Effect of NETD on Detectivity (D^*)

The NETDs are determined from the noise sources in the above section. The NETD affects the detectivity as given by

$$D^* = \frac{4F^2}{\mathrm{NETD} \cdot \tau_0 \frac{dL_B}{dT_s}} \sqrt{\frac{\Delta f}{A_d}},$$

where A_d is the detector area [4]. This expression of detectivity is applicable for radiations emitted by a blackbody ($\varepsilon = 1$) and for detectors of 100% absorbance. dL_B/dT_s is the derivative of the integrated blackbody radiance with respect to source temperature. The overall theoretical detectivity, D_{Th}^*, of the detector system of this study consists of four components: (i) the detectivity of the SiC detector (D_{SiC}^*); (ii) the detectivity due to the interaction between the He–Ne laser and SiC detector ($D_{L,\mathrm{SiC}}^*$); (iii) the detectivity due to the fluctuation in the reflected power of the He–Ne beam arriving at the Si detector ($D_{L,\mathrm{Si}}^*$); and (iv) the detectivity due to the Si detector itself (D_{Si}^*).

The detectivity of the SiC detector, D_{SiC}^*, can be obtained by modifying the above general detectivity expression to account for the absorbance of the SiC detector (α_{SiC}) and the emissivity of the stainless steel radiation source (ε_s):

$$D_{\mathrm{SiC}}^* = \frac{4F^2}{\mathrm{NETD}_{\mathrm{SiC}} \alpha_{\mathrm{SiC}} \varepsilon_s \tau_0 \left(\frac{dL_B}{dT_s}\right)_{\lambda_{12}}} \sqrt{\frac{\Delta f_{\mathrm{SiC}}}{A_{\mathrm{SiC}}}}. \tag{24}$$

The $\mathrm{NETD}_{L,\mathrm{SiC}}$ has been obtained in Eq. (21), and it is due to the noise in the He–Ne laser and SiC detector (see Sections 4.B and 4.E). The $\mathrm{NETD}_{L,\mathrm{SiC}}$ and detectivity, $D_{L,\mathrm{SiC}}^*$, account for the noise mechanism that arises because of changes in the temperature of the SiC detector while the temperatures of the MWIR radiation source and He–Ne laser are kept constant. For this noise mechanism, the detectivity is given by

$$D^*_{L,\mathrm{SiC}} = \frac{\sqrt{A_{\mathrm{Si}}\Delta f_{\mathrm{Si}}}}{\mathrm{NETD}_{L,\mathrm{SiC}}\alpha_{\mathrm{Si}}\rho_{\mathrm{SiC},L}P_L\frac{d\rho_{\mathrm{SiC},L}}{dT_{\mathrm{SiC}}}}. \tag{25}$$

The $\mathrm{NETD}_{L,\mathrm{Si}}$ has been obtained in Eq. (22), and it is due to the noise from the fluctuations in the reflected power of the He–Ne laser beam arriving at the Si detector (Sections 4.C and 4.E). The $\mathrm{NETD}_{L,\mathrm{Si}}$ and detectivity, $D^*_{L,\mathrm{Si}}$, account for the noise mechanism that arises because of changes in the temperature of the He–Ne laser resonator while the temperatures of the MWIR radiation source and SiC detector are kept constant. For this noise mechanism, the detectivity is given by

$$D^*_{L,\mathrm{Si}} = \frac{\sqrt{A_{\mathrm{Si}}\Delta f_{\mathrm{Si}}}}{\mathrm{NETD}_{L,\mathrm{Si}}\frac{dP_L}{dT_L}}. \tag{26}$$

The $\mathrm{NETD}_{\mathrm{Si}}$ has been obtained in Eq. (23), and it is due to the noise of the He–Ne laser detector, which is the Si detector in this study (Sections 4.D and 4.E). The $\mathrm{NETD}_{\mathrm{Si}}$ and detectivity, D^*_{Si}, account for the noise mechanism that arises because of the changes in the temperature of the SiC detector while the temperatures of the MWIR radiation source and He–Ne laser resonator are kept constant. For this noise mechanism, the detectivity is given by

$$D^*_{\mathrm{Si}} = \frac{\sqrt{A_{\mathrm{Si}}\Delta f_{\mathrm{Si}}}}{\mathrm{NETD}_{\mathrm{Si}}\frac{dP_{r,L}}{dT_{\mathrm{SiC}}}}. \tag{27}$$

The total theoretical detectivity can be obtained by the following expression [24]:

$$\frac{1}{D^*_{\mathrm{Th}}} = \sqrt{\left(\frac{1}{D^*_{\mathrm{SiC}}}\right)^2 + \left(\frac{1}{D^*_{L,\mathrm{SiC}}}\right)^2 + \left(\frac{1}{D^*_{L,\mathrm{Si}}}\right)^2 + \left(\frac{1}{D^*_{\mathrm{Si}}}\right)^2}.$$

5. Results and Discussion

A. Optical Response of the SiC Detector at Room Temperature due to Changes in Its Refractive Index and Reflectance caused by the Incident MWIR Wavelength

Four quadrants of the SiC substrate were doped with Ga over a region of 3 mm square in each quadrant. The number of laser passes was varied from one to four to achieve different dopant concentrations in different quadrants, thus resulting in one-, two-, three-, and four-pass samples on the same substrate corresponding to the number of laser passes. Some of the results are for the two-pass sample as a typical case. However, the detectivity and NETD are discussed for the four-pass sample since it provides a better optical signal than the other samples of lower dopant concentrations.

The absorbance, reflectance, and transmittance spectra of the Ga-doped (two-pass sample) and as-received undoped substrates are presented in Figs. 2(a)–2(c). The spectrum of the Ga-doped sample in Fig. 2(a) shows that it has higher absorbance (25%) than that (12%) of the undoped sample at the MWIR wavelength of 4.21 μm. The doped sample exhibits another absorption peak at 4.63 μm. These two peaks were considered for analyzing the detector characteristics because the bandpass filter, which was used to extract the MWIR radiation from the radiation source, allowed transmission in the wavelength range of 4.08–4.81 μm. Several mechanisms may cause such multiple dopant energy levels, such as the substitutional occupancy of the lattice sites of Si and C atoms by the Ga atoms and the strains due to the presence of Ga atoms at the interstitial sites.

Two emission bands are considered around these two absorption peaks to calculate the total radiance (L_T) of the source at the SiC detector surface. One of the bands ranges from 4.2 to 4.29 μm around the peak wavelength at 4.21 μm, while the second band is from 4.54 to 4.66 μm around the peak wavelength at 4.63 μm. The spectral radiance can be calculated as $L_\lambda = \varepsilon_s L_{B\lambda}$, where ε_s is the emissivity of the oxidized stainless steel radiation source with the value $\varepsilon_s = 0.7$ at 1200 K for the wavelengths 4.21 and 4.63 μm [25]. $L_{B\lambda}$ is the spectral radiance of a blackbody given by Planck's theory of blackbody radiation. The total radiance of the source, L_T, is determined by integrating the spectral radiance, L_λ over the two emission bands, and it was found to be $L_T = 0.2\ \mu\mathrm{W/mm^2\ sr}$ at 25°C. Since the source emits more radiation as its temperature increases, its spectral radiance (L_λ) and the radiance in each emission band (L_i, $i = 1$ and 2) increase as shown in Fig. 3(a). The incident irradiance on the detector in each emission band, I_i for $i = 1$ and 2, is determined using L_i and by considering the solid angle subtended by the $\mathrm{CaF_2}$ source lens at the extended radiation source and the diameter of the MWIR irradiation spot formed by the $\mathrm{CaF_2}$ detector lens at its focal plane on the SiC detector. So the total MWIR irradiance that enters into the detector can be written as $I_a = \sum_{i=1}^{2}\alpha_i I_i$, where α_i is the absorbance of the detector in the ith emission band for which the experimental values are 0.32 and 0.30 for the two emission bands around the peak wavelengths at 4.21 and 4.63 μm, respectively. Accordingly, the detector needs to be very sensitive to detect any change in the source temperature. In addition, the EM wave collection optics need to be of a very high quality to collect the maximum amount of waves from the source and focus them onto a small spot on the detector.

The SiC detector reflects the He–Ne beam to produce an optical signal in terms of the power of the reflected He–Ne beam. This reflected power (P_r), which was measured with a silicon-based He–Ne laser detector coupled with a power meter by varying the radiation source temperature from 25°C to 650° C, is presented in Fig. 3(b) as a function of the total radiance of the source. Therefore, P_r represents the optical response of the SiC detector to the MWIR wavelengths of 4.21 and 4.63 μm. This optical response is normalized with respect to the incident

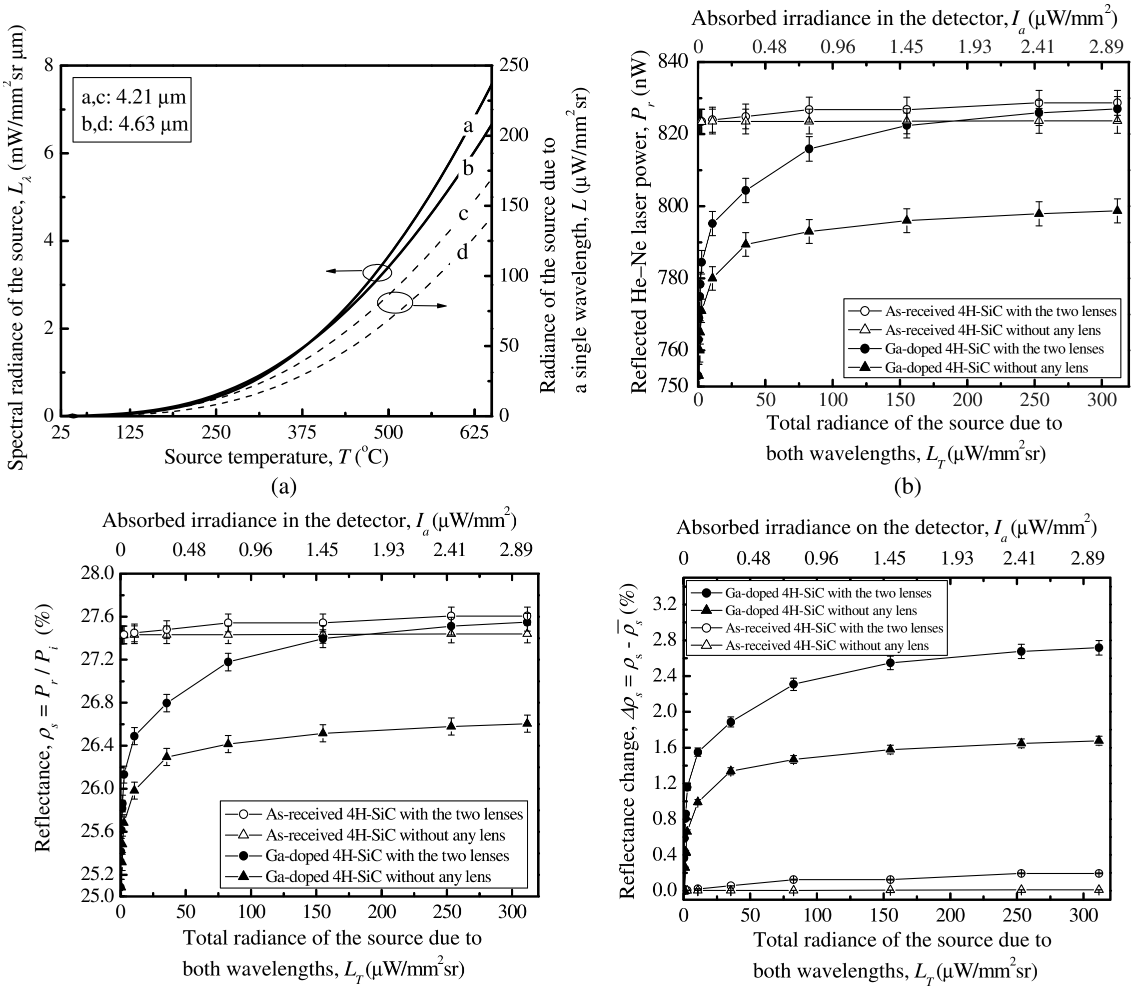

(a) (b) (c) (d)

Fig. 3. Effects of the source radiance on the optical response of the detector (two-pass Ga-doped samples) compared to the as-received (undoped) samples. The data show that the doped samples produce significant optical signals at the He–Ne laser wavelength of 632.8 nm: (a) effect of the source temperature on its radiance at two MWIR wavelengths of 4.21 and 4.63 μm; (b) reflected powers of the He–Ne laser in the presence of the MWIR irradiance; (c) reflectances of the samples at the He–Ne laser wavelength in the presence of the MWIR irradiance (ρ_s, $s = u$ or d); and (d) difference between the reflectance obtained in the presence of the MWIR irradiance and that obtained in the absence of the MWIR irradiance for each sample ($\Delta\rho_s = \rho_s - \bar{\rho}_s$).

He–Ne laser power (P_i) to obtain the reflectance of the SiC detector as $\rho_s = P_r/P_i$, where the subscript $s = u$ for the undoped (as-received) sample and $s = d$ for the doped sample. These results are presented in Fig. 3(c) for two optical arrangements to collect the MWIR radiations from the source and direct them to the detector. It is evident from Figs. 3(b) and 3(c) that the use of lenses improves the optical response of the detector significantly. The effect of the MWIR radiation on the optical response of the detector is examined by determining the change in the reflectance compared to the reflectance of the detector in the absence of the MWIR radiation, i.e., $\Delta\rho_s = \rho_s - \bar{\rho}_s$. Here, $s = u$ or d as defined above, and ρ_s and $\bar{\rho}_s$ are the reflectances of the sth type sample in the presence and absence of MWIR irradiance, respectively. As shown in Fig. 3(d), the change in the reflectance of the doped sample is significant as the temperature of the radiation source increases, while the change is very small for the undoped as-received sample. This improved optical response of the Ga-doped sample is due to more photon flux at elevated temperatures of the radiation source and the presence of Ga acceptor levels corresponding to the quantum of incident energy.

The transmitted powers of the He–Ne beam were also measured for the undoped and doped samples when both the SiC detector and the radiation source were at room temperature. Based on the incident and transmitted powers and the Beer–Lambert law for the transmission of the He–Ne beam through the samples, their absorption coefficients were determined. Using these data, the absorption index of the undoped sample was found to be 1.42×10^{-4} for the He–Ne laser wavelength of 632.8 nm. Similarly, the absorption indices of four Ga-doped samples representing one-, two-, three-, and four-laser passes were found to be 1.50×10^{-4}, 1.53×10^{-4},

1.57×10^{-4}, and 1.60×10^{-4}, respectively, for the He–Ne laser wavelength. These results indicate that the absorption indices are negligibly small. Using the reflectance data and the expression [Eq. (3)] for reflectance due to multiple reflections of the He–Ne beam inside the SiC samples, the refractive indices n_s, $s = u$, and d were calculated for the samples in the presence of MWIR irradiance as presented in Fig. 4(a). The doped sample has a lower refractive index than the undoped sample because of the lower refractive index of the doped sample at room temperature. In the absence of MWIR irradiance, the refractive indices ($\bar{n}_s$) were found to be 3.44, 3.08, 3.17, 3.23, and 3.3 for the undoped and the Ga-doped samples of one-, two-, three-, and four-laser passes, respectively. The changes in the refractive index, $\Delta n_s = n_s - \bar{n}_s$, are presented in Fig. 4(b) for the two-pass sample to illustrate a typical case, which shows that the MWIR photons change the refractive index of the detector significantly compared to that of the undoped sample. It should be noted that the refractive indices ($\bar{n}_d$) increase as the number of laser passes increase. Similarly, the reflectances (ρ_d) were found to be 25.93, 25.02, 24.4, and 23.41% for the four Ga-doped samples of one-, two-, three-, and four-laser passes, respectively, when the radiation source was at room temperature. A higher number of laser passes increases the dopant concentration in the samples as discussed below. A higher dopant concentration enables increasing photoexcited carrier density, which in turn affects the reflectance and refractive index of the doped samples.

Figure 5(a) shows the effect of the source temperature on the photoexcited carrier density, which was determined using

$$N_c(T_s) = \frac{\eta_{e,\mathrm{SiC}} K}{d_d} \frac{\lambda}{hc} \frac{I_a(T_s)}{\alpha_{\mathrm{SiC}}} N_a. \tag{28}$$

$\eta_{e,\mathrm{SiC}} K / d_d$ can be identified as the Einstein transition probability for the transition of carriers from a lower energy level to a higher energy level. K and N_a are a proportionality constant and the acceptor concentration in the Ga-doped SiC detector, respectively [26]. The photoexcited carrier densities (N_c) in the doped samples were calculated using Eq. (28) and a value of $N_a = 6.05 \times 10^{10}\ \mathrm{cm}^{-3}$ for the two-pass sample at $T_s = 25°\mathrm{C}$. Even this relatively low photoexcited carrier density produces a significant optical signal as shown in Fig. 3(b). Figure 5(b) shows the reflectances and refractive indices of the samples at the He–Ne laser wavelength in the presence of the MWIR irradiance for different dopant concentrations. The theoretical reflectances and refractive indices of the detector can be determined using Eq. (3). At higher dopant concentrations, more holes are available in the dopant energy level to accommodate more photoexcited carriers, which results in larger changes in the carrier density. Since more photoexcited carriers can be produced in the sample with a higher dopant concentration, the refractive index increases, and, consequently, its reflectance decreases. Although the theoretical and experimental results are different, they exhibit similar trends. The discrepancy may be due to the misalignment of various optical elements in Fig. 1 and the unstable output power of the He–Ne laser.

B. Evaluation of the Detector Performance

In this study, the experimental data involve the signal-to-noise ratio of two devices, which are the

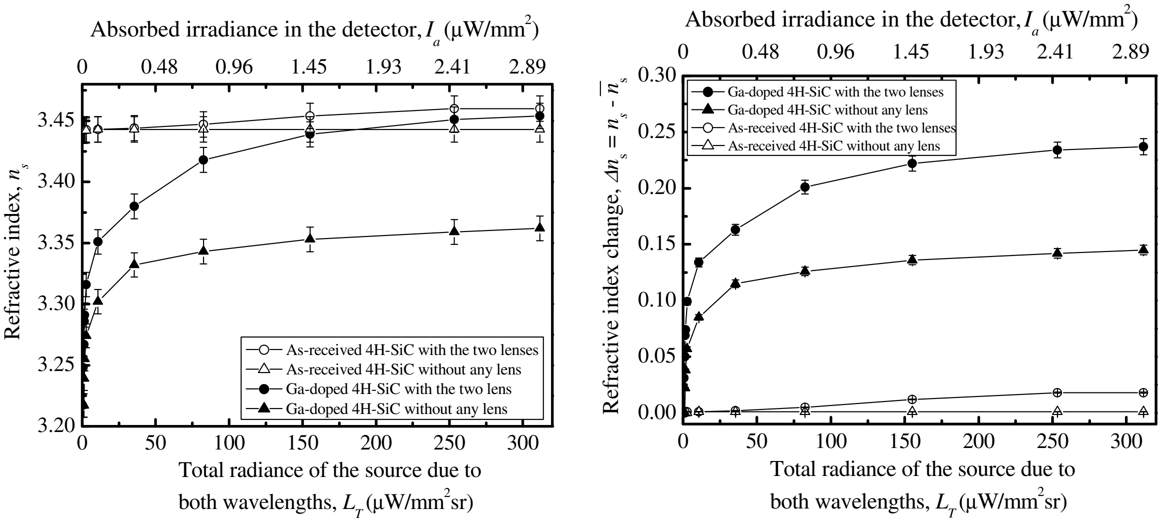

(a) (b)

Fig. 4. Effects of the source radiance on the optical response of the detector (two-pass Ga-doped samples) compared to the as-received (undoped) samples. The data show that the doped samples produce significant optical signals at the He–Ne laser wavelength of 632.8 nm: (a) refractive indices of the samples at the He–Ne laser wavelength in the presence of the MWIR irradiance (n_s, $s = u$ or d) and (b) difference between the refractive index obtained in the presence of the MWIR irradiance and that obtained in the absence of the MWIR irradiance for each sample ($\Delta n_s = n_s - \bar{n}_s$).

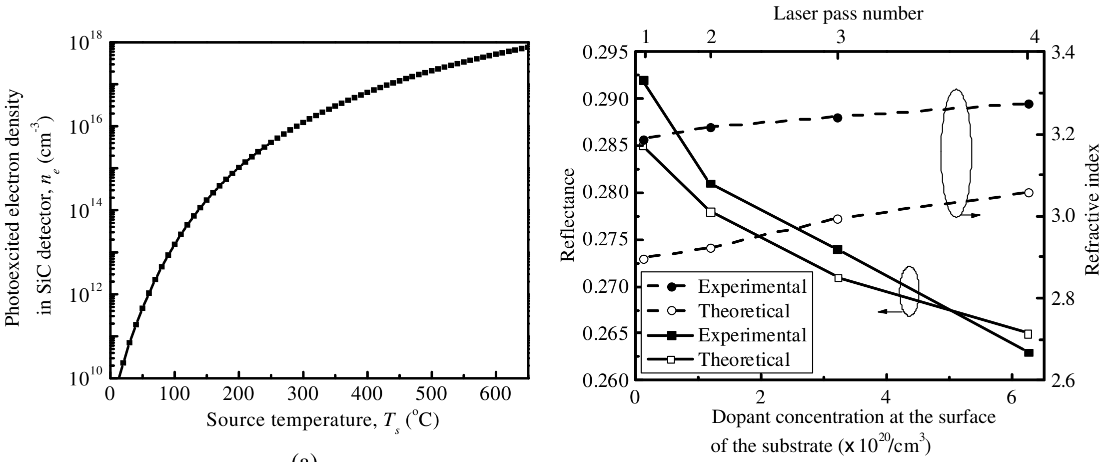

(a)

(b)

Fig. 5. (a) Effect of the source temperature on the free carrier density in the detector (two-pass Ga-doped samples) and (b) reflectances and refractive indices of the samples at the He–Ne laser wavelength in the presence of the MWIR irradiance for different dopant concentrations obtained by scanning the laser for multiple passes as shown on the top axis.

Ga-doped 4H-SiC sample that produces the optical signal by reflecting a He–Ne beam and the Si detector that is used to measure the power of the reflected He–Ne beam. The experimental detectivity of this SiC–Si detector system, which represents the combined effect of the SiC and Si detectors, can be written as [4]

$$D^*_{\mathrm{Exp}} = \frac{S/N}{\rho_{\mathrm{SiC},L} I_{i,L}} \sqrt{\frac{\Delta f_{\mathrm{Si}}}{A_{\mathrm{Si}}}}, \tag{29}$$

where $I_{i,L}$ is the irradiance of the He–Ne laser incident on the SiC detector. The irradiance on the Si detector ($I_{r,L}$) can be related to the reflectance of the SiC MWIR detector by the expression $I_{r,L} = \rho_{\mathrm{SiC},L} I_{i,L}$.

The detectivity of the four-pass sample is calculated using Eq. (29) for the case where both the detector and radiation source are at room temperature (25°C). The signal noise (N), which is the standard deviation of the fluctuations in the output laser power, and the signal (S), which is the average value of the laser power used for calculating N, were found to be $S = 752$ nW and $N = 6.68$ nW based on the He–Ne laser power meter reading on a Si detector. These data yield a signal-to-noise ratio (S/N) of the SiC–Si detector system as 112.62. The time constant of the Si detector was $t_c = 10$ ms, which corresponds [17] to $\Delta f_{\mathrm{Si}} = 1/(2t_c) = 50$ Hz. The other data for the above-mentioned signal and noise measurements are the incident He–Ne laser irradiance on the SiC sample surface as $I_{i,L} = 26.79\ \mathrm{nW/mm^2}$, the reflectance of the sample as $\rho_{\mathrm{SiC},L} = 0.28$ at the He–Ne laser wavelength, and the detector area $A_{\mathrm{Si}} = 1.13\ \mathrm{mm}^2$ for a He–Ne beam with a diameter of 1.2 mm. Substituting these data into Eq. (29), the detectivity of the SiC–Si detector system was found to be $1.07 \times 10^{10}\ \mathrm{cm \cdot Hz^{1/2}/W}$, while the theoretical result was $1.11 \times 10^{10}\ \mathrm{cm \cdot Hz^{1/2}/W}$ based on various noise mechanisms as shown in Table 1.

Similarly, the theoretical detectivities of the SiC–Si detector system were obtained using Eqs. (24)–(27) for different dopant concentrations, and the corresponding theoretical detectivities were calculated

Table 1. Theoretical Values of $NETD_{\mathrm{Th}}$ and Detectivity of the Ga-Doped 4H-SiC IR Detector at 4.21 μm

Detector Components	Noise Sources	Related Equations	$\mathrm{NETD_{Th}}$ (mK)	Detectivity, D^*_{Th} ($\mathrm{cm \cdot Hz^{1/2}/W}$)
Ga-doped 4H-SiC detector	1. Photon shot noise from the radiation source 2. Johnson noise 3. Generation–recombination	(4)–(6), (19), (20), (24)	12.15	4.53×10^{10}
SiC detector + He – Ne laser probe beam	1. Interferometric noise due to multiple reflection and interference of the He–Ne beam in SiC	(7)–(10), (21), (25)	14.88	2.31×10^{10}
He – Ne laser probe beam + Si detector	1. Power noise due to intensity fluctuations 2. Power noise due to frequency fluctuations	(11)–(14), (22), (26)	16.72	2.05×10^{10}
He–Ne laser power meter (Si detector)	1. Photon shot noise from the He–Ne laser 2. Johnson noise 3. Shot noise 4. Generation–recombination	(15)–(18), (23), (27)	19.84	1.73×10^{10}
Total			32.28	1.11×10^{10}

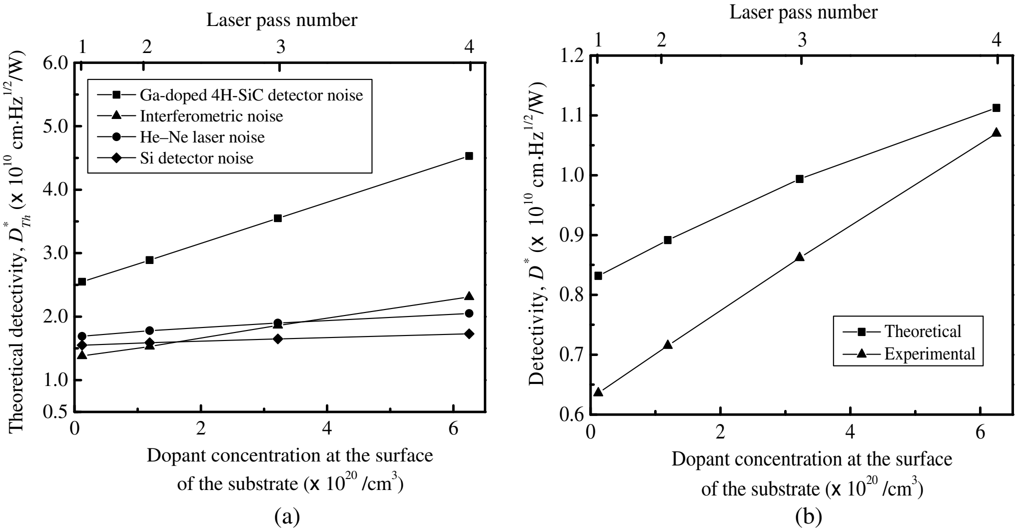

Fig. 6. Effects of dopant concentration on the MWIR detectibility of the SiC detector and comparison between theoretical and experimental results: (a) theoretical detectivity for each noise source and (b) total theoretical and experimental detectivity. The detectivity was determined by keeping the detector and radiation source at 25°C each.

as listed in Table 1. Figure 6(a) shows how the theoretical detectivity depends on different noise mechanisms as the dopant concentration is varied, and the discrepancy between the theoretical and experimental results are presented in Fig. 6(b). This discrepancy may be due to several reasons such as the misalignment of different optical elements in Fig. 1 and loss of the optical signal due to the scattering of the He–Ne beam in these elements including SiC. The loss of photoexcited carriers due to diffusion and the absorption and scattering in various defect sites in the SiC substrate can also contribute to the discrepancy.

The NETD is another figure of merit defining the smallest temperature difference between two points of a source that a detector can image distinguishably. It represents the temperature of a source above the background (ambient) temperature that produces a signal in the detector equal to the RMS of the detector noise. The $\mathrm{NETD_{Exp}}$ can be determined as the ratio of the standard deviation of the detector signal (σ_n) to the system intensity transfer function (SITF) [27]. σ_n can be expressed as

$$\sigma_n = \sqrt{\left[N\sum_{i=1}^{N}(P_i)^2 - \left(\sum_{i=1}^{N}P_i\right)^2\right]/(N(N-1))}$$

by incorporating Bessel's correction to the conventional definition of the standard deviation [28], where P_i, $i = 1, 2, 3, \ldots N$, is the ith value of the optical signal, i.e., the power of the reflected He–Ne beam. The reflected power was measured at different times to obtain N signals for the same source temperature. The SITF of the detector can be obtained by considering $\mathrm{SITF} = (\bar{P}_s - \bar{P}_{\mathrm{BG}})/(T_s - T_{\mathrm{BG}})$, where $\bar{P}_s$ and $\bar{P}_{\mathrm{BG}}$ are the average reflected powers of the He–Ne beam at the source and background

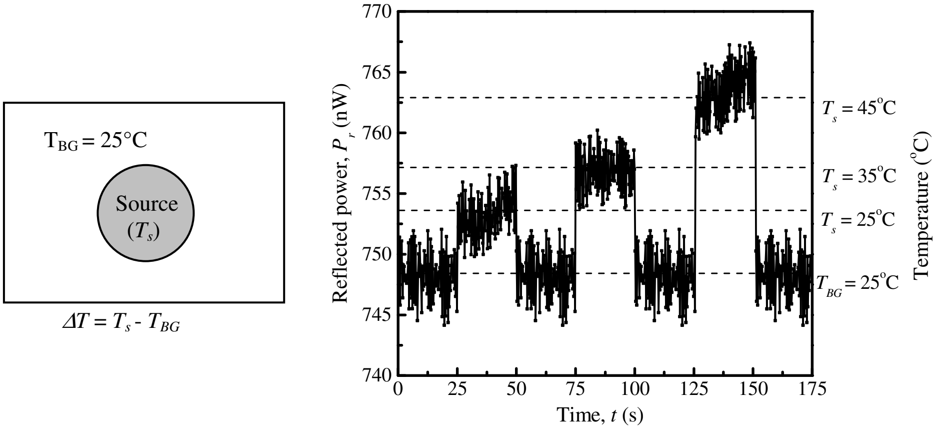

Fig. 7. Reflected powers of the He–Ne beam at room temperature and at higher temperatures of the source to determine NETD. T_{BG} is the background temperature of other materials surrounding the source. It is 25°C in this study, and the reflected power is lower than that of the source because of the difference in emissivity.

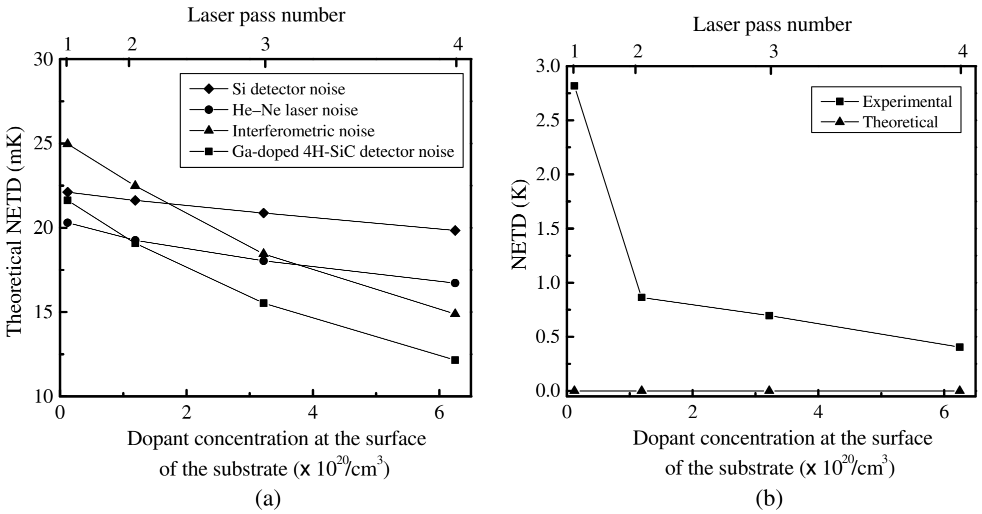

Fig. 8. Effects of dopant concentration on the MWIR detectibility of the SiC detector and comparison between theoretical and experimental results: (a) theoretical $\mathrm{NETD_{Th}}$ for each noise source and (b) total theoretical and experimental ($\mathrm{NETD_{Exp}}$) values of NETD. $\mathrm{NETD_{Exp}}$ was obtained by keeping the detector at 25°C and the radiation source at 35°C and 45°C.

temperatures T_s and T_{BG} over N_s and N_{BG} number of data points, respectively. It should be noted that T_s and T_{BG} need to be chosen properly [29] so that $T_s - T_{\mathrm{BG}} \neq 0$. In this study, the stainless steel radiation source was kept at three temperatures equaling 25°C, 35°C, and 45°C and the power of the reflected He–Ne beam was measured at each temperature. Typical data for the reflected power are presented in Fig. 7. One hundred values ($N = 100$) of the reflected power were chosen arbitrarily for each temperature to determine $\mathrm{NETD_{Exp}}$.

The average values of the reflected power for the four-pass sample are $\bar{P}_{r,1} = 752\ \mathrm{nW}$, $\bar{P}_{r,2} = 756\ \mathrm{nW}$, and $\bar{P}_{r,3} = 767\ \mathrm{nW}$ at $T_s = 25°\mathrm{C}$, 35°C, and 45°C, respectively, and the corresponding standard deviations are $\sigma_1 = 0.9\ \mathrm{nW}$, $\sigma_2 = 0.51\ \mathrm{nW}$, and $\sigma_3 = 0.9\ \mathrm{nW}$. Using two pairs of data at 25°C and 35°C, and at 35°C and 45°C, the SITFs are obtained as $\mathrm{SITF}_{12} = 0.599\ \mathrm{nW/K}$ and $\mathrm{SITF}_{13} = 0.126\ \mathrm{nW/K}$, respectively, and the corresponding values of $\mathrm{NETD_{Exp}}$ are $\mathrm{NETD}_{12} = 1505\ \mathrm{mK}$ and $\mathrm{NETD}_{13} = 404\ \mathrm{mK}$. Similarly, experimental results were used to determine the $\mathrm{NETD_{Exp}}$ of other samples (one-, two-, and three-pass samples) for different dopant concentrations and the $\mathrm{NETD_{Exp}}$ was found to vary from 1.505 K to 404 mK as the dopant concentration increases from 1.15×10^{19} to $6.25 \times 10^{20}\ \mathrm{cm}^{-3}$, respectively. For the four-pass sample, however, the theoretical $\mathrm{NETD_{Th}}$ was found to be 25.3 mK based on the noise mechanisms listed in Table 1. These results are presented in Figs. 8(a) and 8(b). Figure 8(a) shows the effect of different noise mechanisms on the theoretical $\mathrm{NETD_{Th}}$ as a function of the dopant concentration in SiC. Figure 8(b), on the other hand, compares the experimental $\mathrm{NETD_{Exp}}$ with the theoretical results. The difference between the theory and experiment may be due to the same reasons as those in the case of detectivity.

6. Conclusion

An n-type 4H-SiC substrate has been doped with Ga using a laser doping technique and the doped sample operates as an uncooled optical photodetector in the MWIR range. The detector produces optical signals in contrast to the electrical signals produced by conventional electrical photodetectors. The dopant concentration was varied to examine the effects of dopant concentration on the detectivity and NETD of the optical photodetector. Since the signal-to-noise ratio affects the detectivity and NETD, the noise mechanisms in various components of the detector system have been analyzed theoretically. Four major noise sources are (i) interaction of the incident MWIR photons with the doped SiC sample, (ii) He–Ne laser power noise due to intensity and frequency fluctuations, (iii) interference of the He–Ne beam due to multiple reflections inside the doped SiC sample, and (iv) interaction of the reflected He–Ne laser with the Si detector. For the MWIR wavelengths at 4.21 and 4.63 μm, the experimental detectivity of the optical photodetector is $1.07 \times 10^{10}\ \mathrm{cm \cdot Hz^{1/2}/W}$ based on experimental data in the case of the sample doped with Ga using four laser passes, while the theoretical value is $1.11 \times 10^{10}\ \mathrm{cm \cdot Hz^{1/2}/W}$ when both the detector and radiation source were at 25°C. The corresponding experimental and theoretical values of NETD are 404 mK and 15.5 mK, respectively. The discrepancy between the experimental and theoretical results may be due to the misalignment of various optical elements, optical signal loss due to the scattering of the He–Ne beam, and photoexcited carrier loss due to diffusion, absorption, and scattering in the SiC substrate.

Appendix A

The rate of change of free carrier density can be obtained by

$$\left\{\begin{matrix}\text{Rate of change of}\\ \text{free carrier density}\end{matrix}\right\} = \left\{\begin{matrix}\text{Rate of generation of}\\ \text{free carrier density}\end{matrix}\right\} - \left\{\begin{matrix}\text{Rate of loss of}\\ \text{free carrier density}\end{matrix}\right\}.$$

The photoexcited rate of free carriers within the doped SiC detector per unit volume depends on the absorbed irradiance I_a, the internal quantum efficiency $\eta_{i,\mathrm{SiC}}$, the detector area A_{SiC}, and the photon energy $h\nu_M$, as $(I_a \eta_{i,\mathrm{SiC}} A_{\mathrm{SiC}}/h\nu_M V)$. The photo-generated carriers decay based on their recombination lifetime τ_r, and this decay is approximated as $\Delta N_c/\tau_r$. The other term of free carrier loss is by diffusion. The free carriers are diffusing into the detector area A_{SiC} with the diffusivity D at a diffusion rate of $DA_{\mathrm{SiC}}(\Delta N_c/l_D)$, which represents the number of photoexcited carriers diffusing per unit time, where the diffusion length (l_D) is expressed as $l_D \approx \sqrt{4D\tau_d}$ for two-dimensional diffusion [30]. The characteristic diffusion time is τ_d before recombination occurs, and τ_d is taken as the MWIR irradiation time. The rate of free carrier loss by diffusion per unit volume is written as $(\Delta N_c A_{\mathrm{SiC}}/V)\sqrt{D/4\tau_d}$, which becomes $\Delta N_c/d_d \sqrt{D/4\tau_d}$ by considering the detector volume V as the product of the detector area and the depth of the doped region (d_d).

This work was supported by the Naval Undersea Warfare Center (NUWC) Division, Newport, Rhode Island, U.S.A., Strategic Internal Investment FY: 2009.

References

1. D. Scribner, J. Schuler, P. Warren, J. Howard, and M. Kruer, "Image preprocessing for the infrared," Proc. SPIE **4028**, 222–233 (2000).
2. M. Reine, "Review of HgCdTe photodiodes for IR detection," Proc. SPIE **4028**, 320–330 (2000).
3. M. Schlessinger, *Infrared Technology Fundamentals* (Marcel Dekker, 1995).
4. E. L. Dereniak and G. D. Boreman, *Infrared Detectors and Systems* (Wiley, 1996).
5. J. Piotrowski and A. Rogalski, "Uncooled long wavelength infrared photon detectors," Infrared Phys. Technol. **46**, 115–131 (2004).
6. S. J. Lee, Y. H. Lee, S. H. Suh, Y. J. Oh, T. Y. Kim, M. H. Oh, C. J. Kim, and B. K. Ju, "Uncooled thermopile infrared detector with chromium oxide absorption layer," Sens. Actuators A **95**, 24–28 (2001).
7. P. Muralt, "Micromachined infrared detectors based on pyroelectric thin films," Rep. Prog. Phys. **64**, 1339–1388 (2001).
8. M. Noda, K. Hashimoto, R. Kubo, H. Tanaka, T. Mukaigawa, H. Xu, and M. Okuyama, "A net type of dielectric bolometer mode of detector pixel using ferroelectric thin film capacitors for infrared image sensor," Sens. Actuators A **77**, 39–44 (1999).
9. F. Niklaus, C. Vieider, and H. Jakobsen, "MEMS-based uncooled infrared bolometer arrays: a review," Proc. SPIE **6836**, 68360D (2007).
10. P. G. Datskos, N. V. Lavrik, and S. Rajic, "Performance of uncooled microcantilever thermal detectors," Rev. Sci. Instrum. **75**, 1134–1148 (2004).
11. Z. Guo, Q. Zhang, F. Dong, D. Chen, Z. Xiong, Z. Miao, C. Li, B. Jiao, and X. Wu, "Performance analysis of microcantilever arrays for optical readout uncooled infrared imaging," Sens. Actuators A **137**, 13–19 (2007).
12. M. F. Toy, O. Ferhanoglu, H. Torun, and H. Urey, "Uncooled infrared thermo-mechanical detector array: design, fabrication and testing," Sens. Actuators A **156**, 88–94 (2009).
13. P. R. Chalker, "Wide bandgap semiconductor materials for high temperature electronics," Thin Solid Films **343–344**, 616–622 (1999).
14. P. G. Neudeck, "Progress towards high temperature, high power SiC devices," in *Compound Semiconductors 1994, Institute of Physics Conference Series Number 141, Proceedings of the Twenty-first International Symposium on Compound Semiconductors*, San Diego, Calif. (Institute of Physics, 1994), pp. 1–6.
15. G. Lim and A. Kar, "Effect of laser scans on the diffusion depth and diffusivity of gallium in n-type 4H-SiC during laser doping," Mater. Sci. Eng., B **176**, 660–668 (2011).
16. G. Lim, T. Manzur, and A. Kar, "Optical response of laser-doped silicon carbide for an uncooled midwave infrared detector," Appl. Opt. **50**, 2640–2653 (2011).
17. E. L. Dereniak and D. G. Crowe, *Optical Radiation Detectors* (Wiley, 1984).
18. M. Rubin, "Solar optical properties of windows," Energy Research **6**, 123–133 (1982).
19. J. L. Gimlett and N. K. Cheung, "Effects of phase-to-intensity noise conversion by multiple reflections on gigabit-per-second DFB laser transmission systems," J. Lightwave Technol. **7**, 888–895 (1989).
20. K. Petermann, *Laser Diode Modulation and Noise* (Kluwer, 1988).
21. A. Yariv, *Quantum Electronics* (Wiley, 1989).
22. F. Riehle, *Frequency Standards: Basics and Applications* (Wiley-VCH, 2004).
23. D. Grbovic, N. V. Lavrik, S. Rajic, S. R. Hunter, and P. G. Datskos, "Nano-mechanical Infrared Detectors," in Encyclopedia of Nanoscience and Nanotechnology, H. S. Nalwa, ed. (American Scientific Publishers, to be published).
24. G. Lim, T. Manzur, and A. Kar, "Improved optical properties and detectivity of uncooled silicon carbide mid-wave infrared detector with increased dopant concentration," J. Opt. **14**, 105601 (2012).
25. R. Siegel and J. Howell, *Thermal Radiation Heat Transfer* (Taylor and Francis, 1994), pp. 60–131.
26. J. Mazumder and A. Kar, *Theory and Application of Laser Chemical Vapor Deposition* (Plenum, 1995).
27. Y. Li, D. Pan, C. Yang, and Y. Luo, "NETD test of high-sensitivity infrared camera," Proc. SPIE **6723**, 67233Q (2007).
28. W. H. Beyer, *Handbook of Mathematical Sciences* (CRC, 1975).
29. J. M. Lloyd, *Thermal Imaging Systems* (Plenum, 1975), pp. 166–184.
30. D. B. Dusenbery, *Living at Micro Scale: The Unexpected Physics of Being Small* (Harvard University, 2009).